

Structural studies of biarylpyridines fluorophores lead to the identification of promising long wavelength emitters for use in fluorescent chemosensors

A. G. Fang, J. V. Mello and N. S. Finney*

Department of Chemistry and Biochemistry, University of California, San Diego, 9500 Gilman Dr., La Jolla, CA 92093-0358, USA

Received 15 April 2004; revised 24 June 2004; accepted 19 August 2004

Available online 22 September 2004

Abstract—Fluorescent chemosensors—molecules whose fluorescence emission changes in response to a reversible binding event—require both a substrate binding domain and a reporting fluorophore. Our approach to chemosensor development is based on a combination of a new signaling mechanism and a modular fluorophore synthesis. The latter feature has facilitated detailed study of the properties of polyarylpyridine fluorophores, and has led to the identification of a visibly-emissive pyridine as a promising lead structure for chemosensor development. The results of this study are described herein.

© 2004 Elsevier Ltd. All rights reserved.

1. Introduction

Fluorescent chemosensors—molecules whose fluorescence emission changes in response to a reversible binding event—require a substrate binding domain, a reporting fluorophore and a signaling mechanism that allows the two to communicate. We have previously described the development of fluorescent chemosensors that rely on conformational restriction as signaling mechanism.^{1–4} This effort was driven by the hypothesis that it would combine two important and often mutually-exclusive features of other systems: simplicity of molecular architecture and generality of signaling mechanism. While we have conducted extensive photophysical studies on chemosensors based on biphenyl and biarylacetylene fluorophores, the most promising of our systems are the biarylpyridine, which exhibit several of desirable properties:

- (1) Visible emission from a locally excited (LE) state that is highly responsive to ion-binding induced conformational restriction.
- (2) A second, longer-wavelength visible emission band arising from a charge transfer (CT) state induced by coordination of an ion to the pyridine nitrogen.
- (3) Modular synthetic assembly.

- (4) Tuning of the emission wavelength by remote substituents on the pyridine ring.

The simple architecture of these systems is self-evident (Fig. 1).² The generality of the signaling mechanism is attested to by the perfect correlation between metal–ion binding detected by ¹H NMR and observed fluorescence response—in all cases to date, ion binding produces a detectable change in fluorescence emission.

In parallel with efforts to widen the variation of ligand structure, we have synthesized numerous new arylpyridine fluorophores with the objective of shifting both LE and CT emission further into the visible region.² We provide here a detailed description of these efforts, including identification of important structure–emission relationships, discovery of a potentially serious limitation to our fluorophore design, and a solution to this problem guided by an understanding of structure–emission relationships.

2. Background

Fluorescent chemosensors allow fluorescence detection, with all the associated benefits, of non-fluorescent analytes.¹ The importance of fluorescent chemosensors in applications as diverse as environmental monitoring, cellular imaging and biomedical device construction is increasingly widely appreciated. The majority of established chemosensors fall into one of 3 categories:

- (1) Systems based on direct interaction between the analyte

Keywords: Fluorescence; Chemosensor; Pyridine; Synthesis; Spectroscopy.

* Corresponding author. Present address: Organisch-chemisches Institut, Universität Zürich, Winterthurer-strasse 190, CH-8057 Zürich, Switzerland. Tel.: +41 (01) 635 4283; e-mail: finney@unizh.ch

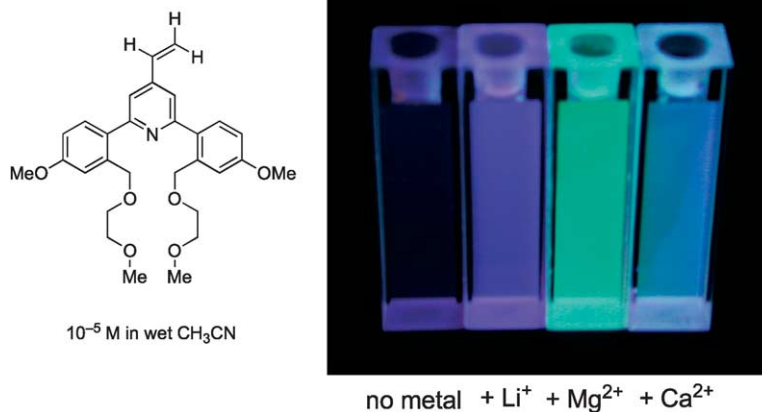


Figure 1. An arylpyridine fluorescent chemosensor with dual visible emission.

- (almost always a metal ion) and a nitrogen atom lone pair that is ‘wired into’ the fluorophore (Fig. 2-1).^{1,5}
- (2) Systems in which analyte binding displaces a fluorophore or changes its microenvironment (Fig. 2-2).^{1,6}
 - (3) Systems in which analyte binding alters the energy transfer between a fluorophore/acceptor pair, where the acceptor is either another fluorophore or a quencher (Fig. 2-3).^{1,7,8}

The first category, which represents the statistical majority of reported fluorescent chemosensors, has the significant advantage of relying on relatively simple molecular architecture. Important examples of this approach include Ca^{2+} - and Zn^{2+} -responsive chemosensors with applicability for cellular imaging.^{5c,d} The central limitation of this approach is the requirement for

lone-pair coordination. This generally constrains the substrate scope to metal ions and dictates that the fluorophore/receptor hybrid contain benzylic or anilinic nitrogen atoms, which in turn restricts the design of new fluorophores and/or binding domains.

In contrast, the third category, often based on fluorescence resonant energy transfer (FRET) between donor and acceptor fluorophores, typically relies on substantially complex molecular architecture—polypeptides, oligonucleotides or fusion proteins.^{7,8} Important embodiments of this strategy include fusions of green fluorescent protein (GFP) analogs and calmodulin that can be expressed *in vivo* to facilitate Ca^{2+} imaging in cells.^{7a} Offsetting the limitation of complexity is the generality of the signaling mechanism, which places no constraint on the structure of the binding

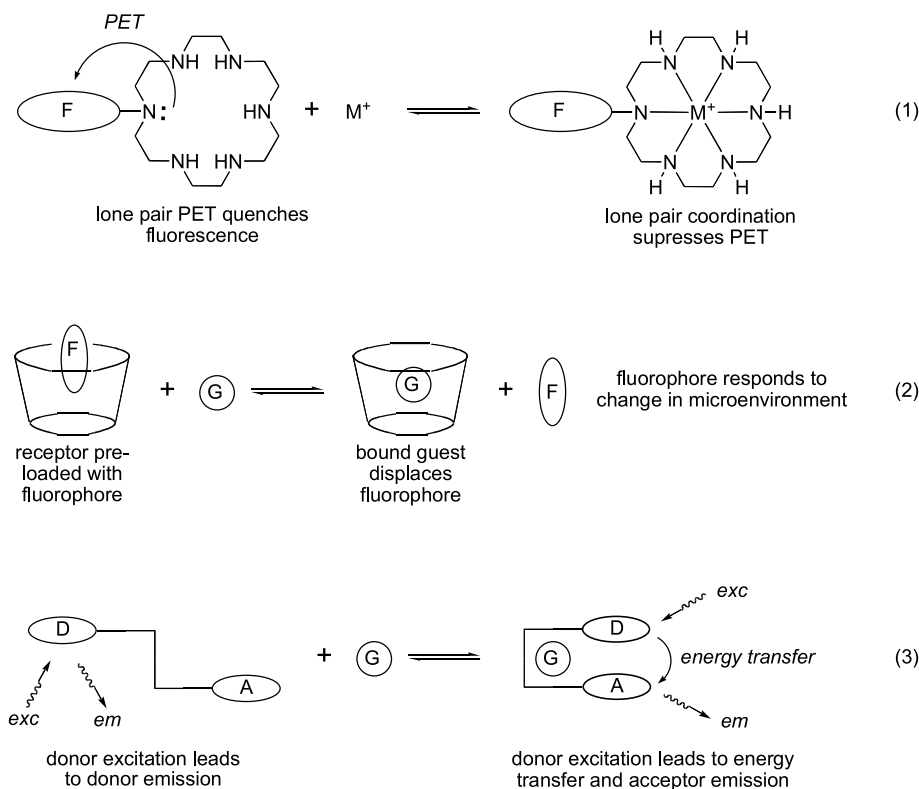


Figure 2. Broad overview of fluorescent chemosensor strategies.

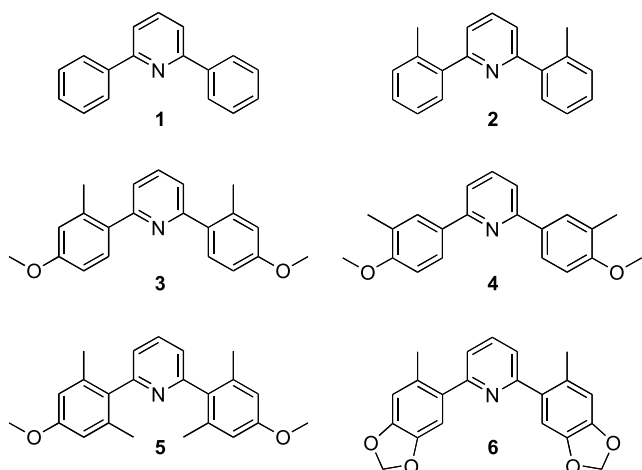


Figure 3. Biarylpyridines with varying substituents at the 2 and 6-positions.

domain beyond a requirement that binding induce a large change in interchromophore distance.

The second category, initially based primarily on displacement of covalently-tethered fluorophores from the cavity of cyclodextrin hosts, are appropriately intermediate between the first and third categories in terms of complexity and generality.⁶ Embodiments typically rely on structures no more complicated than cyclodextrin, and generality is limited only by the requirement that there be sufficient similarity between the fluorophore and the analyte that the analyte can effectively compete with the fluorophore in binding to the receptor. Important recent examples of this strategy include systems for sensing ATP.^{6b}

3. Results

3.1. Structural studies on ‘fourth category’ fluorophores

Fluorescent chemosensors based on conformational

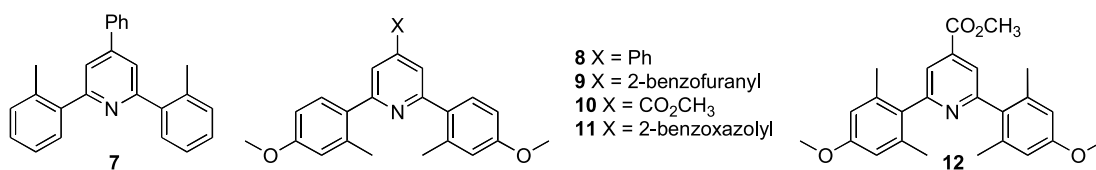


Figure 4. Biarylpyridines with varying substituents at the 4-position.

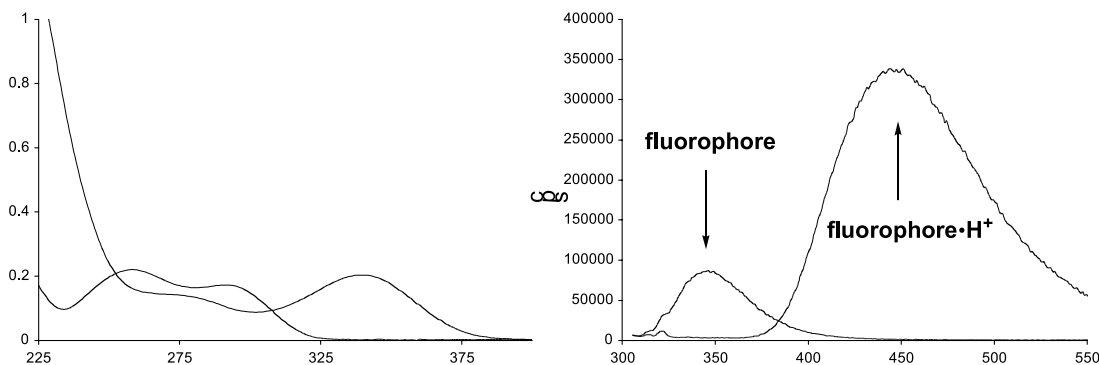


Figure 5. Absorption and emission spectra of the chemosensor from Figure 1.

restriction represent a fourth category addition to the above list. As mentioned above, the modular nature of biarylpyridine fluorophores (our preferred member of this fourth category) simplifies structure–property studies.² The goals of the present work were gaining a greater understanding of substituent effects and red-shifting the LE and CT emission wavelengths. We initially focused on the nature of the aryl substituents at the 2- and 6-positions (Fig. 3), and subsequently investigated fluorophores with varied 4-substituents in greater detail (Fig. 4). With regard to LE and CT emission, the default emission of biarylpyridines is that from the LE state. However, CT emission can be induced by simple protonation of the pyridine (Fig. 5). For both states, the longest wavelength absorption maximum correlates with the excitation maximum for fluorescence emission. In cases where the CT state is non-emissive (vide infra) the formation of the CT state can still be verified by characteristic changes in the absorption spectrum (Fig. 5).

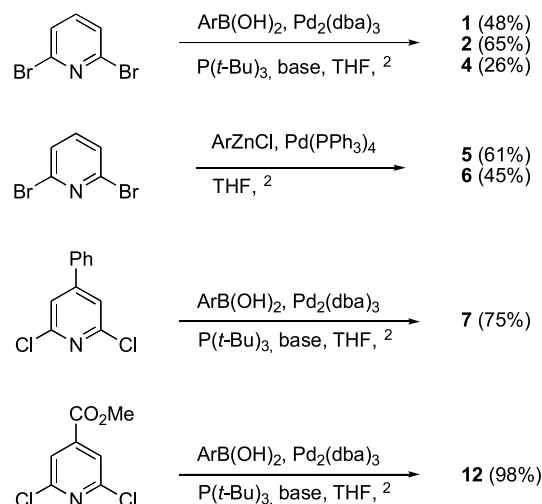
3.2. Synthesis of arylpyridine fluorophores

The syntheses of compounds 3 and 8–11 have been described previously.² Fluorophores 1, 2 and 4–6 were prepared from 2,6-dibromopyridine, while 7 and 12 were prepared from 2,6-dichloro-4-phenylpyridine and 2,6-dichloro-4-carboxymethylpyridine, respectively (Scheme 1). Central to all of these syntheses is the efficiency of palladium catalyzed cross coupling of the required halopyridines.^{2,9,10}

4. Discussion

4.1. Influence of the 2,6-substituents on optical properties

Our first generation biarylpyridine chemosensors (cf. Fig. 1) all contained as common features *o,o'*-alkyl and *p,p'*-OCH₃ substituents on the aryl groups at the 2 and 6 positions. The presence of the *o,o'* groups was presumed to be essential



Scheme 1. Synthesis of arylpyridine fluorophores.

based on our previous study of biphenyl systems. However, the properties of biarylpyridines and biphenyls are sufficiently different that this presumption warranted direct evaluation. The *p,p'*-substituents were initially included based on the ready availability of the precursor aryl fragments rather than deliberate design, and the inclusion of these groups even more clearly required evaluation.

The spectroscopic properties of **1–6** (Table 1) reveal that both the alkyl and OCH₃ substituents are essential to the function of our system. The inclusion of the *o,o'*-alkyl substituents is essential for lowering the LE quantum yield to the point where it is subject to modulation by conformational restriction. For instance, the fluorophore in Figure 1 has an LE quantum yield of ~0.02; in contrast, fluorophores with LE quantum yields >0.10 no longer respond strongly to binding-induced conformational restriction. (This is one of the ironies inherent in an approach based on using substrate binding to turn a poor fluorophore into a good fluorophore—it is essential to start with a poor fluorophore.) The presence of the polarizing OCH₃ substituents provides a desirable red-shift in absorption and emission but what would be, in the absence of the alkyl substituents, an undesirable increase in LE quantum yield.

The addition of *o,o'*-CH₃ groups to 2,6-biphenylpyridine (**1** vs **2**) leads to a slight reduction in extinction coefficient and quantum efficiency of emission from both the LE and CT

states. The reduction in LE emission parallels that seen when comparing biphenyl ($\phi=0.18$) to the more twisted derivative 2,2'-dimethylbiphenyl ($\phi=0.01$).¹¹ Based on previous work with biphenyls, we conclude that this reduction in quantum yield is in large part due to the increased efficiency of spin-orbit coupling (SOC) in twisted biaryl excited states.¹² While factors independent of biaryl torsion might be considered, such as C–C twisting and C–H stretching-mediated deactivation of the excited state, the similarity of the quantum yields of biphenyl and 3,3'-dimethylbiphenyl ($\phi=0.21$) argues against this.¹¹ The 'gap rule'—the empirical observation that the rate of IC decreases as excited state energy increases—also argues against this possibility, in that the excited state energy is in excess of 100 kcal/mol.^{3a,13,14} An additional consequence of introducing *o,o'*-CH₃ groups is an undesirable blue shift in both the LE (20 nm) and CT (5 nm) emission. This is also consistent with reduced planarity and thus reduced conjugation in the excited state.

The addition of *p,p'*-OCH₃ substituents (**2** vs **3**) has a dramatic impact on the efficiency of both absorption and emission, almost completely compensating for the reduction in quantum yield caused by introduction of the *o,o'*-CH₃ groups. In addition, it has a pronounced effect on the absorption and emission wavelengths. Notably, the emission maximum for the LE state shifts more than 20 nm to the red, while that of the CT state shifts by more than 60 nm. The emission shifts are accompanied by smaller but still significant red shifts in the LE and CT excitation maxima. These indicate that both the LE and CT excited states are highly polarized, with the flanking aromatic rings serving as electron donors and the pyridine ring, consistent with its electron deficient nature relative to a hydrocarbon, serving as an electron acceptor. While this polarization is present in the ground state, it is clearly more pronounced in the excited states: the near doubling of ϵ reflects a large increase in the transition dipole for the excitation from ground to excited state.¹⁵ A corresponding increase in the efficiency of radiative decay of the LE state, shown by the increase in ϕ , is expected based on the proportionality of the Einstein A and B coefficients (which govern emission and excitation) for fluorophores of very similar structure.¹⁶ The red shifts in emission wavelength indicate that the *p*-OCH₃ groups serve to stabilize both the LE and CT excited states, effectively lowering their energy and reducing the energy gap between excited and ground state. The effects on absorption and emission are much more pronounced in the CT state, as

Table 1. Salient optical properties of **1–6**

Compound	ϵ ($\times 10^3$) ^a	Φ (LE) ^{a,b}	Φ (CT) ^c	LE _{exc} ^d	LE _{em} ^e	CT _{exc} ^f	CT _{em} ^g
1	10.2	0.037	0.951	302	338	322	393
2	8.1	0.004	0.831	280	320	307	388
3	14.8	0.031	0.177	290	352	342	449
4	11.6	0.560	0.544	315	359	366	459
5	9.3	0.003	0.021	272	342	324	450
6	13.5	0.059	0.004	303	378	359	480

^a Measured at LE excitation maximum.

^b Quantum yield of LE emission.

^c Quantum yield of CT emission.

^d Excitation maximum for LE state.

^e Emission maximum for LE state.

^f Excitation maximum for CT state.

^g Emission maximum for CT state.

expected based on its greater charge separation relative to the LE state.

The importance of the *o,o'*-CH₃ groups is underscored by comparison to the corresponding *m,m'*-dimethyl case (**3** vs **4**). Relocation of the flanking CH₃ groups lowers the absorptivity of the molecule while simultaneously increasing the LE quantum yield by an order of magnitude and doubling the CT quantum yield. In addition, the excitation maxima for the *m,m'* isomer are significantly red shifted, although there are only very small changes in the emission wavelengths. The decreased absorptivity indicates that removal of the *o,o'*-CH₃ groups leads to greatly increased conjugation—and thus polarization—in the ground state, while the smaller changes in the emission wavelengths indicate smaller changes in the degree of polarization in the excited state. The lower value of ϵ for **4** is thus explained, as ϵ should scale with the transition dipole which should in turn vary with the difference in polarization of the ground and excited states.¹⁵ That is, increasing the polarization of the ground state without altering the polarization of the transition state would be expected to decrease ϵ , in the absence of other effects. The smaller red shifts in the emission wavelengths are consistent with greater excited state planarization, and the effect of removing the *o,o'*-CH₃ groups is similar in comparing **3** vs **4** and **2** vs **1**.

The influence of deplanarization is further delineated by the addition of a second pair of flanking CH₃ groups (**3** vs **5**). While deplanarization and polarization offset one another in **3**, in **5** deplanarization almost fully compensates for the ground state influence of polarization, and the values for ϵ (reduced by $\sim 4 \times 10^{-3}$) and the absorption maxima (reduced by ~ 20 nm) of **5** are even lower than those of **2**, which lacks both the OCH₃ and additional CH₃ groups. Similarly, the quantum yield of both the LE and CT states descend to values similar to those of **2**. The emission maxima provide valuable structural information. The wavelength of LE emission shows a ~ 20 nm blue shift relative to **3**, while that the CT emission remains unchanged within measurement error. This indicates that the ground and LE states of **5** are less planar and thus less conjugated than those of **3**, as would be expected based on increased steric congestion. That this congestion does not influence the CT emission wavelength suggests that the CT state is

twisted, such that the additional CH₃ groups have relatively little influence on the conformation and thus energetic separation of the CT state and the corresponding twisted conformation of the ground state. While this evidence is indirect, it is consistent with the extensive literature on twisted intramolecular charge transfer (TICT) states.^{17,18}

There are two significant aspects of the spectroscopic properties of bis(piperonyl) compound **6**. First, the further increase in polarization induced by two additional alkoxy substituents (**6** vs **3**) leads to the longest LE and CT emission wavelengths in the series (380 and 480 nm, respectively, compared to 350 and 450 nm for **3**).¹⁹ Second, and of great practical importance, emission from **6** is a presage of a trend that is more fully illustrated by **7–12**: as emission from biarylpyridines moves farther to the red, the quantum yield of the CT state begins to drop off. The first of these observations may be rationalized much as the difference between **2** and **3**, with electron donating substituents stabilizing the polarized excited states and reducing the energetic separation from the ground state. The second and more problematic observation is again consistent with the gap rule.¹⁴ For **6**, the 480 nm CT emission is equivalent to an energy gap of almost exactly 60 kcal/mol, which correlates with significant decrease in CT quantum yield ($\phi = 0.06$, vs 0.28 for **3**). This energy (ca. 60 kcal/mol) is apparently the upper limit at which IC begins to contribute to nonradiative decay.

4.2. Influence of the 4-substituent on optical properties

The influence of the 4-substituent on the emission of biarylpyridines is delineated by compounds **7–12** (Table 2). Three prominent trends can be seen. First, increasing the chromophore surface or polarization by substitution at the 4-position can lead to a significant red shift in LE emission, and in one case can alter the identity of the core fluorescing unit. Second, the quantum yield for LE emission increases as emission moves to longer wavelengths. Third, CT emission decreases over the same series, leading quickly to molecules with non-emissive CT states.

By itself, comparison of 2,6-bis(*o*-tolyl)pyridine and its 4-phenyl counterpart (**7** vs **2**) would suggest that the 4-substituent has a modest influence on most of the properties

Table 2. Salient optical properties of **7–12** (with **2**, **3** and **5** for comparison)

Compound	$\epsilon (\times 10^3)^a$	Φ (LE) ^b	Φ (CT) ^c	LE _{exc} ^d	LE _{em} ^e	CT _{exc} ^f	CT _{em} ^g
7	4.9	0.005	0.803	295	349	302	399
8	9.3	0.200	0.182	310	379	350	483
9	38.3	0.210	0.016	310	400	370	505
10	4.4	0.230	—	324	424	379	—
11	14.6	0.140	—	300	440	—	—
12	4.7	0.070	—	300	457	360	—
2	8.1	0.004	0.051	280	320	307	388
3	14.8	0.031	0.282	290	352	342	449
5	9.3	0.003	0.021	272	342	324	450

^a Measured at LE absorption/excitation maximum.

^b Quantum yield of LE emission.

^c Quantum yield of CT emission.

^d Excitation maximum for LE emission.

^e Emission maximum for LE excitation.

^f Excitation maximum for LE state.

^g Emission maximum for CT excitation.

of these fluorophores. The quantum yields are virtually identical, the extinction coefficient is actually slightly reduced, and the emission wavelengths for the LE and CT states shift to longer wavelength by 30 and 15 nm, respectively. The longer emission wavelength is expected based on the increase in fluorophore surface area, thus delocalization and stabilization of the excited state. It is not immediately obvious why the LE emission wavelength responds more strongly than the CT state to the increased delocalization, or why the CT quantum yield responds more strongly than that of the LE.

Addition of a 4-phenyl group to the chromophore bearing both *o*-CH₃ and *p*-OCH₃ groups (**3**) leads to a much more dramatic change in spectroscopic properties (**8** vs **3**). The extinction coefficient decreases, indicative of a lower transition dipole that presumably results from an increase in ground state polarization relative to the LE state. The LE quantum yield increases substantially ($\phi=0.20$ vs $\phi=0.03$ for **3**) while the CT quantum yield decreases ($\phi=0.09$ vs $\phi=0.28$ for **3**). Absorption and emission wavelengths for both states shift to longer wavelength, the LE emission now approaching the visible region of the spectrum. The reduced CT emission efficiency is a consequence of the gap rule, as described above. The increased LE efficiency must result from the extended conjugation of the chromophore surface, and we take this as evidence that the 2,6-substituents—and their conformation mediated nonradiative decay—contribute less, proportionally, to the properties of more extended chromophores. (This is substantiated by **9** and **11**; vide infra.)

Replacing the phenyl group with a benzofuran provides further evidence that increased chromophore delocalization diminishes the impact of nonradiative decay mediated by the 2,6-aryl substituents (**9** vs **3**). Extension with benzofuran leads to a large increase in extinction coefficient, a further increase in LE quantum yield and a further reduction in CT quantum yield. In addition, the LE emission maximum moves into the visible region (400 nm), and the CT emission maximum moves from green into the green-yellow (505 nm). The emission and quantum yield effects may be rationalized as were those for **8**. The near quintupling of extinction coefficient is surprising but, like the increased LE quantum yield, shows that the 4-substituent makes an increased contribution to the character of the excited state. This can be seen most readily by comparing the absorption spectra of **8** and **9** (Fig. 6). The

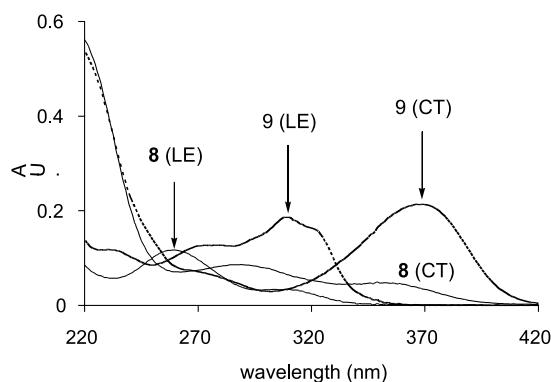


Figure 6. Absorption spectra of **8** and **9**.

absorption spectrum of **8** is similar to that of **3** and the 4-vinyl derivative (Fig. 3). Immediate differences in peak shape and the number and relative intensity of the absorption maxima can be seen for **9**. This demonstrates that the benzofuran substituent is a powerful determinant of the nature of the excited states, with commensurate deemphasis of the 2,6-aryl groups.

Installation of a benzoxazole at the 4-position yields a chromophore with absorption properties that no longer resemble those of **1–10** (Fig. 7), and the absorption and emission of which do not change noticeably upon addition of excess TFA. This structural variation has thus altered the fluorophore identity to the point that a CT excited state—radiative or nonradiative—simply no longer exists.

As a counterpart to increasing the chromophoric surface, placing a methyl carboxylate (which extends conjugation by only 2 atoms) at the 4-position shows that direct polarization of the pyridine, like polarization of the 2,6-biaryl groups, also influences fluorophore behavior (**10** vs **3**). The extinction coefficient decreases, consistent with a more polarized ground state and less difference in polarization between the ground and excited states. The LE emission becomes slightly more efficient and moves further into the visible, the 425 nm maximum representing a 100 nm Stokes shift. The CT state—which can still be observed by absorbance—is non-emissive.

The final variant on 4-substitution, **12**, is the tetramethyl analog of **10**. It is notable in that while it has a shorter wavelength LE absorption, as would be predicted by sterically decreased conjugation, it has a longer emission wavelength. The red shifted emission, which corresponds to ~ 62 kcal/mol, now runs afoul of the gap rule and accounts for the reduced quantum yield. That a longer emission wavelength results from increased deplanarization suggests that the optimal conformation of the LE state is no longer as near planar as was the case for **3**. Although this suggests an optimal geometry more suited to the CT state, which is nonradiative and expected to be twisted, the CT state can clearly be identified by the absorption spectrum and is distinct from the LE state. The apparent change in optimal LE state geometry remains unexplained, but coupled with the reduced quantum yield it provides an opportunity for the development of fluorescent chemosensors with visible

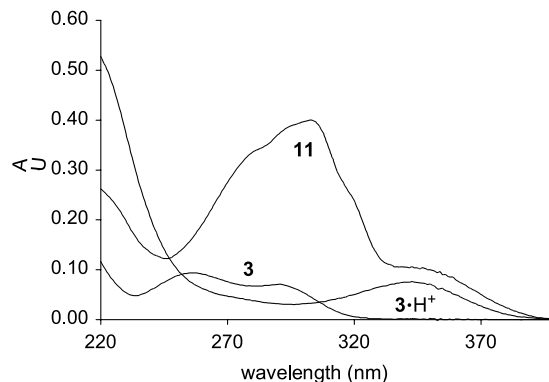


Figure 7. Comparison of the absorption spectra of **3** and **11**.

emission and geometrical constraints different from those associated with **3**.

4.3. The limitations of longer wavelength fluorophores

The properties of the pyridine fluorophores with visible LE emission constitute a potential problem for the development of fluorescent chemosensors based on conformational control. The approach hinges on being able to start with a poor fluorophore and induce increased LE emission efficiency via binding induced conformational restriction. This, in turn, means the approach is best suited for fluorophores with low initial quantum yields—unlike the visibly-emissive **8–11**. In addition, the loss of the second signaling channel—the CT emission—is a setback, in that dual emission provided an additional level of discrimination for distinguishing between bound metal ions.

The first of these concerns, reduced sensitivity at longer LE emission wavelength, is ameliorated to an extent by the observation that **13**, the 4-carboxymethyl analog of the chemosensor shown in Figure 1, still provides a visible response to the presence of metal ions (Fig. 8). The ~4-fold increase in emission intensity translates to a $\phi \geq 0.90$, which is a record among the systems we have studied, and is easily observed by eye. Offsetting this promising result are the lack of response to Mg^{2+} and Ca^{2+} (cf. Fig. 1), which had previously induced formation of the radiative CT state. While treatment with TFA indicates that $\mathbf{13} \cdot \text{H}^+$ possesses a nonemissive CT state, neither Mg^{2+} nor Ca^{2+} induce formation of this state, indicating that the pyridine ring is now sufficiently electron deficient that the nitrogen atom serves as a poor Lewis base. Related studies with the podand derived from the 4-phenyl fluorophore (**9**) showed only minimal metal ion response, an observation which suggests that the response of **13** to Li^+ is the exception rather than the rule. That said, it is worth noting that **13** still provides a visible emissive readout of the presence of Li^+ .

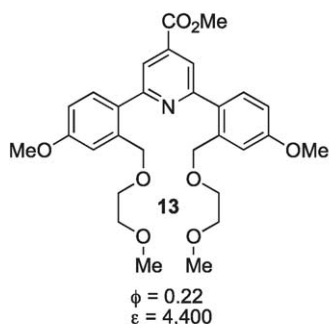
5. Conclusion and recent progress

In summary, variation of the substituents at the 2, 4 and 6-positions of polyaryl pyridines can have a profound effect

on the absorbance and emission of these fluorophores. With regard to the 2,6-aryl groups, *o,o'*-alkyl substitution was shown to be essential for maintaining low initial quantum yields, while *p,p'*-alkoxy substitution was shown to provide a beneficial red shift in emission without untoward increase in emission efficiency. The influence of the 4-substituent on absorption and emission wavelengths was dramatic, with LE emission in the green region of the visible spectrum being possible. An unfortunate side effect of increased LE and CT emission wavelengths is the accompanying variation in quantum yields. LE emission efficiency (ideally low) increases with wavelength, while CT emission efficiency (ideally high) decreases with wavelength. While in certain cases we have found that fluorescent chemosensors with relatively high initial quantum yields (e.g., $\phi = 0.23$ for **13**) retain useful metal ion response, this is not generally the case.

Two recent observations represent promising leads for the development of the next generation of pyridine-derived fluorescent chemosensors. The first of these arose from juxtaposing the 4-carboxylate substituent found in **10** and **13** with the 4-vinyl group found in the chemosensor from Figure 1. By preparing vinylogous amide **14** (Fig. 9), we have found a fluorophore that benefits from a red shift induced by the carboxylate substituent, but does not suffer from the increase in quantum yield seen in **10** or **13**. The second, and more belated, observation is that the importance of the *p,p'*-methoxy groups may have been overestimated. Podand **15**—similar to **13** and the podand of Figure 1—responds strongly to presence of metal ions (Fig. 10). While the absence of the methoxy groups leads to emission wavelengths that are much shorter than desirable, the lower initial quantum yield ($\phi \leq 0.01$) allows for a much greater dynamic range for the fluorescence response.

Our ongoing efforts focus on gaining a greater understanding the properties of **14**, exploiting this fluorophore for the development of fluorescent chemosensors, and turning the luminescence of long wavelength CT emission back on. In addition, based on evaluation of **15**, it is clearly necessary to reinvestigate the influence of the 4-substituent in the series of fluorophores lacking the *p,p'*-methoxy groups.



no metal + Li^+ + Mg^{2+} + Ca^{2+}

Figure 8. Titration of **13** (10^{-5} M in CH_3CN) with Li^+ .

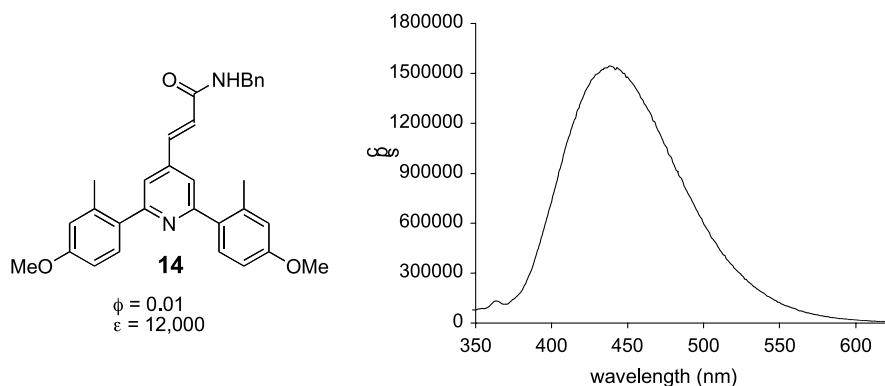


Figure 9. Vinylogous amide **14** has desirable visible LE emission.

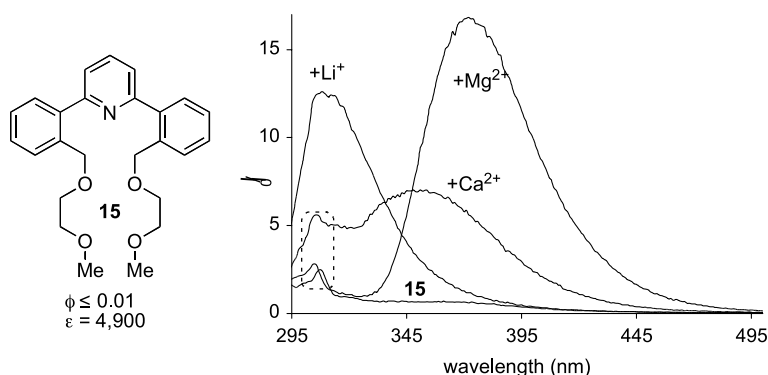


Figure 10. Titration of podand **15** (10^{-5} M in CH_3CN) with metal ions. Emission maxima in broken box are Raman scattering from CH_3CN .

6. Experimental

6.1. General notes

Melting points were obtained in open capillary tubes with a Thomas Scientific Uni-Melt melting point apparatus and are uncorrected. ^1H NMR spectra were obtained on Varian HG-400 (400 MHz) spectrometers. Chemical shifts (δ) are reported in parts per million (ppm) relative to residual solvent (CHCl_3), s, δ , 7.26). Multiplicities are given as: s (singlet), d (doublet), t (triplet), q (quartet), dd (doublet of doublets), ddd (doublet of doublet of doublets), dt (doublet of triplets) and m (multiplet). Proton-decoupled ^{13}C NMR spectra were obtained on Varian HG-400 (100 MHz) spectrometers. ^{13}C chemical shifts are reported relative to CDCl_3 (t, δ , 77.0). IR stretches are given in cm^{-1} ; spectra were obtained on a Nicolet 550 Series II Spectrophotometer. MALDI-FT mass spectroscopic analyses were provided by the facility at The Scripps Research Institute; all other mass spectroscopic analyses were provide by the facility at UCLA.

Fluorescence measurements were carried out in spectroscopic grade CH_3CN on a PTI Quantmaster 2000, with flash lamp excitation and 2 nm excitation and emission slit widths. Solutions of fluorophore were prepared by successive dilution and were typically 1×10^{-5} M in CH_3CN . Solutions of metal perchlorate salts were prepared by successive dilution and were typically 1 M. Fluorescence titrations were carried out by sequentially adding 0.005 or 0.010 mL aliquots of metal solution via micropipette to 2.500 mL of fluorophore solution in a quartz cuvette. The

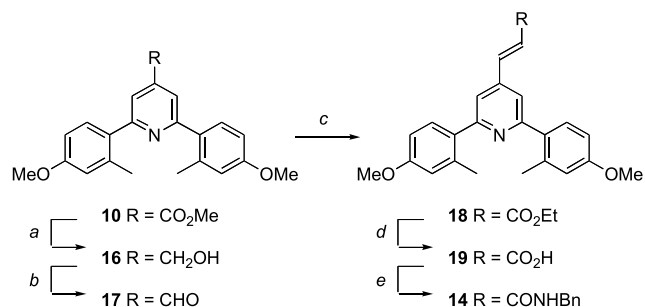
solutions were equilibrated by stirring prior to acquiring fluorescence spectra. No efforts were made to exclude water or air. Quantum yields and extinction coefficients were determined by standard methods.²⁰

Chromatographic purifications were performed by flash chromatography with silica gel (Fisher Scientific, 32–63 μm) packed in glass columns; eluting solvent for each purification was determined by thin layer chromatography (TLC). Analytical TLC was performed on glass plates coated with 0.25 mm silica gel 60 F₂₅₄ (EM Science) using UV light for visualization.

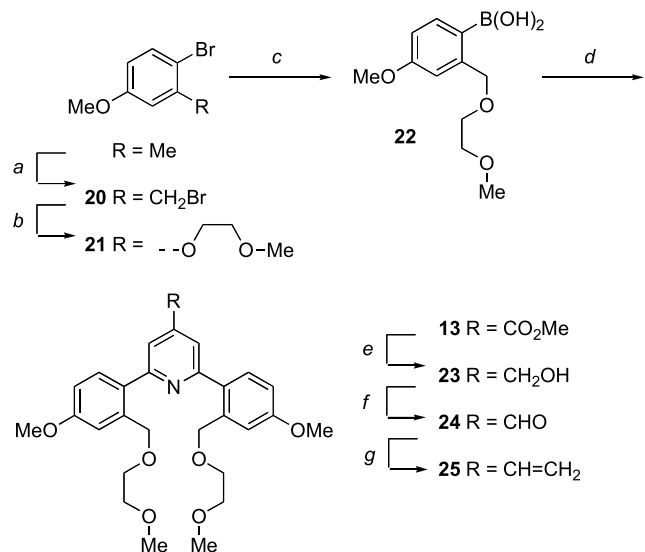
Synthetic procedures were carried out under an inert atmosphere, using standard Schlenk line techniques. Where noted, solutions were degassed by evacuating and backfilling with N_2 several times. THF, CH_2Cl_2 , and benzene were dried by passage through a column of activated alumina.²¹ Pyridine was distilled from CaH_2 . All other reagents and solvents were used as received unless otherwise specified.

6.2. Experimental procedures^{9,10}

Compounds **3** and **8–11** were prepared as described previously.² Compound **1** is commercially available but was prepared as described below for convenience. Compound **14** was prepared in 5 steps and good yield from ester **10** (Scheme 2). Compound **13** and the fluorescent chemosensor shown in Figure 1 (**25**) were prepared from 2-bromo-5-methoxytoluene (Scheme 3). Compound **15** was prepared in analogy to **2** by variation of the boronic acid.



Scheme 2. Preparation of vinylogous amide **14**. Reagents and conditions: (a) DiBAL/THF, -78°C , 89%; (b) DMSO, (COCl)₂, NEt₃, CH₂Cl₂, -78°C , 94%; (c) (EtO)₂P(O)CH₂CO₂Et, ^tBuO⁻K⁺, THF, 0°C , 100%; (d) LiOH·2H₂O, THF, RT 85%; (e) BnNH₂, DEPBT, THF, RT, 94%.



Scheme 3. Preparation of **13** and the chemosensor from Figure 1 (**25**). Reagents and conditions: (a) NBS, AIBN, PhH, 86%;² (b) CH₃OCH₂CH₂OCH₂OH, NaH, THF, 80%; (c) BuLi, B(OⁱPr)₃, THF; NaOH, 70%; (d) 2,6-dichloro-4-carboxy-methylpyridine, Pd₂(dba)₃, P^tBu₃, CsF, THF,² 52%; (e) DiBALiH, THF, -78°C , 99%; (f) DMSO, (COCl)₂, NEt₃, CH₂Cl₂, -78°C , 90%; (g) Ph₃PCH₃⁺I⁻, BuLi, THF, 0°C , 60%.

6.2.1. Compound 1. 2,6-Dibromopyridine (0.100 g, 0.422 mmol, 1 equiv), phenylboronic acid (0.155 g, 1.27 mmol, 3.00 equiv), [HP^tBu₃]⁺BF₄⁻ (0.012 g, 0.040 mmol, 0.10 equiv), Pd₂(dba)₃ (0.019 g, 0.021 mmol, 0.050 equiv), and CsCO₃ (0.756 g, 2.320 mmol, 5.50 equiv) was suspended in THF (10 mL). The reaction mixture was degassed and refluxed for 16 h. After cooling to room temperature, H₂O (50 mL) was added and the mixture extracted with methylene chloride (2×50 mL). The combined organic extracts were dried over Na₂SO₄ and concentrated. Purification by column chromatography (20% toluene/hexanes) produced 0.098 g (0.422 mmol, 48%) of **1** as a white solid, mp $78\text{--}80^{\circ}\text{C}$. ¹H NMR (400 MHz, CDCl₃): δ = 8.18 (m, 4H), 7.82 (dd, 6.8, J = 7.0 Hz, 1H), 7.71 (d, J = 7.6 Hz, 2H), 7.52 (m, 4H), 7.46 (m, 2H). IR (KBr): ν = 3056, 2925, 1588, 1449, 758, 697. TLC (R_f) = 0.11 (20% toluene/hexanes).

6.2.2. Compound 2. Procedure as for **1**, except P^tBu₃ in THF was used as the phosphine source. White solid, mp $68\text{--}70^{\circ}\text{C}$, 65%. ¹H NMR (400 MHz, CDCl₃): δ = 7.81 (t, J = 7.6 Hz, 1H), 7.45 (m, 2H), 7.36 (d, J = 7.6 Hz, 2H), 7.27

(m, 6H), 2.43 (s, 6H). ¹³C NMR (100 MHz, CDCl₃): δ = 159.24, 140.48, 136.11, 135.62, 130.50, 129.67, 128.01, 125.67, 121.83, 20.69. IR (KBr): ν = 3030, 2951, 1562, 1457, 767. HRMS (EI): calcd for C₁₉H₁₆N [M⁺] 259.1361; found 259.1349. TLC (R_f) = 0.4 (5% acetone/hexanes).

6.2.3. Compound 4. Procedure as for **2**. White solid, mp $140\text{--}141^{\circ}\text{C}$, 26%. ¹H NMR (400 MHz, CDCl₃): δ = 7.95 (m, 4H), 7.72 (t, J = 7.6 Hz, 1H), 7.56 (d, J = 8.0 Hz, 2H), 6.94 (d, J = 8.8 Hz, 2H), 3.91 (s, 6H), 2.34 (s, 6H). ¹³C NMR (100 MHz, CDCl₃): δ = 158.42, 156.41, 136.95, 131.74, 129.16, 126.56, 125.50, 117.06, 109.82, 55.47, 16.58. IR (KBr): ν = 2943, 1615, 1562, 1510, 1449, 1256, 1143, 1029. HRMS (EI): calcd for C₂₁H₂₁NO₂ [M⁺] 319.1572; found 319.1569. TLC (R_f) = 0.20 (10% EtOAc/hexanes).

6.2.4. Compound 5. 4-Bromo-3,5-dimethylanisole (0.25 g, 1.17 mmol, 2.00 equiv) was cooled to -78°C in THF (5 mL). *n*-BuLi (1.22 mL 1.20 M in hexanes, 1.46 mmol, 2.50 equiv) was added dropwise and stirred at -78°C for 15 min. ZnCl₂ (0.40 g, 2.92 mmol, 5.00 equiv) was transferred via cannula into the reaction mixture as a THF solution (10 mL), and the reaction was stirred for an additional 15 min. The reaction mixture was transferred via cannula into a flask containing 2,6-dibromopyridine (0.14 g, 0.58 mmol, 1 equiv) and Pd(PPh₃)₄ (0.03 g, 0.03 mmol, 0.05 equiv). The reaction mixture was degassed then refluxed for 20 h. The reaction was allowed to cool to room temperature, H₂O (25 mL) was added, and the mixture was extracted with EtOAc (3×25 mL). The combined organic fractions were washed with brine (1×25 mL), dried over Na₂SO₄, filtered, and concentrated under vacuum. Purification by column chromatography (20% EtOAc/hexanes) produced 0.09 g (0.27 mmol, 46%) of **5** as a pale yellow solid, mp $167\text{--}168^{\circ}\text{C}$. R_f = 0.24 (20% EtOAc/hexanes). IR (KBr): ν = 2961, 1602, 1575, 1463, 1315, 1194, 1160, 1074, and 838 cm⁻¹. ¹H NMR (CDCl₃): δ = 7.80 (t, J = 8 Hz, 1H), 7.17 (d, J = 8 Hz, 2H), 6.64 (s, 4H), 3.80 (s, 6H), and 2.06 ppm (s, 12H). ¹³C NMR (CDCl₃): δ = 159.7, 158.7, 137.1, 136.4, 122.7, 112.9, 112.7, 55.2, and 20.7 ppm. HRMS (DEI): calculated for C₂₃H₂₄NO₂ (M - H⁺): 346.180704, found 346.181374.

6.2.5. Compound 6. 2-Bromo-4,5-methylenedioxytoluene (0.25 g, 1.16 mmol, 3.00 equiv) was cooled to -78°C in THF (5 mL). *n*-BuLi (0.67 mL/1.8 M, 1.20 mmol 3.10 equiv) was added and the reaction stirred for 5 min, ZnCl₂ (0.181 g, 1.65 mmol, 3.50 equiv) in THF (3.0 mL) was added. The arylzinc chloride so generated was transferred via cannula into a degassed solution of 2,6-dibromopyridine (0.0920 g, 0.387 mmol, 1 equiv), Pd₂(dba)₃ (0.018 g, 0.019 mmol, 0.050 equiv, P^tBu₃ (0.56 mL, 0.14 M in THF, 0.077 mmol, 0.20 equiv), and refluxed for 16 h. Upon cooling to room temperature, the reaction mixture was diluted with EtOAc (1×50 mL), washed with H₂O (1×250 mL) and saturated NaCl (1×50 mL). The organic layer was dried over Na₂SO₄, concentrated, and chromatographed on silica gel (10% EtOAc/hexanes) to afford a white solid (0.047 g, 35%), mp $149\text{--}151^{\circ}\text{C}$. ¹H NMR (400 MHz, CDCl₃): δ = 7.75 (t, J = 7.6 Hz, 1H), 7.28 (d, J = 7.6 Hz, 2H), 6.96 (s, 2H), 6.74 (s, 2H), 5.95 (s, 4H), 2.33 (s, 6H). ¹³C NMR (100 MHz, CDCl₃): δ = 158.83, 147.20, 145.50, 135.98, 133.73, 129.43, 121.75, 110.45, 109.91, 100.85, 20.59. IR

(KBr): $\nu=2925, 1562, 1510, 1449, 1047, 933$. HRMS (EI): calcd for $C_{21}H_{16}NO_4 [(M-H)^+]$ 346.1079; found 346.1084. TLC (R_f)=0.20 (12% EtOAc/hexanes).

6.2.6. Compound 7. Procedure as for **2**. White solid, mp 129–130 °C, 75%. 1H NMR (400 MHz, $CDCl_3$): $\delta=7.72$ (dd, $J=1.6, 6.8$ Hz, 2H), 7.60 (s, 2H), 7.51 (m, 5H), 7.29 (m, 6H), 2.48 (s, 3H). ^{13}C NMR (100 MHz, $CDCl_3$): $\delta=159.84, 148.55, 140.51, 138.27, 135.71, 130.52, 129.67, 128.95, 128.85, 128.07, 126.95, 125.68, 119.94, 20.75$. IR (KBr): $\nu=3039, 2925, 1588, 1545, 1396, 767$. HRMS (EI): calcd for $C_{25}H_{20}N [(M-H)^+]$ 334.1596; found 334.1592. TLC (R_f)=0.34 (5% EtOAc/hexanes).

6.2.7. Compound 12. 4-Bromo-3,5-dimethylanisole (0.25 g, 1.17 mmol, 2.00 equiv) was cooled to -78 °C in THF (5 mL). *n*-BuLi (1.22 mL 1.2 M in hexanes, 1.46 mmol, 2.5 equiv) was added dropwise and stirred at -78 °C for 15 min. $ZnCl_2$ (0.40 g, 2.92 mmol, 5.00 equiv) was transferred via cannula into the reaction mixture as a THF solution (10 mL), and the reaction was stirred for an additional 15 min. The reaction mixture was transferred via cannula into a flask containing 2,6-dichloroisonicotinic acid methyl ester (0.120 g, 0.58 mmol, 1 equiv) and $Pd(PPh_3)_4$ (0.03 g, 0.03 mmol, 0.05 equiv). The reaction mixture was degassed then refluxed for 16 h. The reaction was allowed to cool to room temperature, H_2O (25 mL) was added, and the mixture was extracted with EtOAc (3×25 mL). The combined organic fractions were washed with brine (1×25 mL), dried over Na_2SO_4 , filtered, and concentrated under vacuum. Purification by column chromatography (20% EtOAc/hexanes) produced 0.02 g (0.06 mmol, 10%) of **12** as a yellow solid, mp 189 °C. $R_f=0.20$ (20% EtOAc/hexanes). IR (KBr): $\nu=2960, 1732, 1607, 1439, 1396, 1345, 1316, 1245, \text{ and } 1157$ cm^{-1} . 1H NMR ($CDCl_3$): $\delta=7.75$ (s, 2H), 6.64 (s, 4H), 3.96 (s, 3H), 3.80 (s, 6H), and 2.05 ppm (s, 12H). ^{13}C NMR ($CDCl_3$): $\delta=165.7, 160.9, 158.9, 138.1, 137.0, 132.7, 122.1, 112.8, 55.3, 52.8, \text{ and } 20.7$ ppm. HRMS (DEI): calculated for $C_{25}H_{26}NO_4 (M-H)^+$: 404.186184, found 404.187089.

6.2.8. Compound 13. Procedure as for **1** except **22** was used as the boronic acid, P^iBu_3 in THF as the phosphine and CsF as the base. Colorless oil, 52%. 1H NMR (400 MHz, $CDCl_3$): $\delta=7.99$ (s, 2H), 7.54 (d, 2H, $J=8.4$ Hz), 7.20 (d, 2H, $J=2.8$ Hz), 6.93 (dd, 2H, $J=2.8, 8.4$ Hz), 4.72 (s, 4H), 3.98 (s, 3H), 3.87 (s, 6H), 3.57–3.54 (m, 8H), 3.35 (s, 6H). ^{13}C NMR (100 MHz, $CDCl_3$): $\delta=165.83, 160.12, 159.22, 142.50, 137.73, 131.55, 131.42, 120.07, 114.26, 113.45, 71.85, 71.40, 69.61, 59.17, 55.42, 52.73$. IR (neat): $\nu=2890, 1737$ (s), 1606, 1248, 1099. HRMS (MALDI): calcd for $C_{29}H_{36}NO_8 [(M-H)^+]$ 548.2255; found 548.2271. TLC (R_f)=0.20 (45% EtOAc/hexanes).

6.2.9. Compound 14. Carboxylic acid **19**, (0.054 g, 0.139 mmol, 1 equiv), *N,N'*-diisopropyl-*N*-ethylamine (0.048 mL, 0.278 mmol, 2.00 equiv), and 3-(diethoxyphosphoryloxy)-1,2,3-benzotriazin-4(3*H*)-one (DEPBT)²² (0.083 g, 0.278 mmol, 2.00 equiv) was suspended in THF (2.5 mL). After stirring for 5 min, benzylamine (0.018 mL, 0.167 mmol, 1.20 equiv) was added and the resulting solution was stirred for 3 h at 23 °C. The solution was diluted with CH_2Cl_2 (50 mL) and washed with H_2O ($2 \times$

50 mL), and saturated NaCl (1×25 mL). The organic phase was dried over Na_2SO_4 and was concentrated. Purification by flash column chromatography (30% EtOAc/hexanes) provided 0.063 g (0.131 mmol, 94%) of a yellow solid. 1H NMR ($CDCl_3$): $\delta=7.69$ (d, 1H, $J=15.6$ Hz), 7.35 (m, 9H), 6.82 (m, 4H), 6.60 (d, 1H, $J=15.6$ Hz), 5.98 (t, 1H, $J=5.6$ Hz), 4.60 (d, 2H, $J=5.6$ Hz), 3.84 (s, 6H), 2.44 (s, 6H). IR (KBr): $\nu=3283$ (b), 2934, 1676 (s), 1615, 1239, 1047, 741. HRMS (EI): calcd for $C_{31}H_{30}N_2O_3 [M^+]$ 478.2256; found 478.2266. TLC (R_f)=0.33 (35% EtOAc/hexanes).

6.2.10. Compound 15. Procedure as for **1**. Pale yellow viscous oil, 90%. 1H NMR (400 MHz, CD_3CN): $\delta=7.89$ (t, 1H, $J=7.6$ Hz), 7.57 (s, 2H), 7.54 (m, 4H), 7.42 (m, 4H), 4.62 (s, 4H), 3.49–3.39 (m, 8H), 3.23 (s, 6H). ^{13}C NMR (100 MHz, $CDCl_3$): $\delta=158.28, 140.10, 136.50, 135.99, 129.92, 129.00, 128.39, 127.59, 122.23, 71.86, 71.11, 69.41, 58.96$. IR (neat): $\nu=2895, 1731, 1579, 1442, 1107$. HRMS (EI): calcd for $C_{25}H_{29}NO_4 [M^+]$ 407.2097; found 407.2086. TLC (R_f)=0.30 (30% acetone/hexanes).

6.2.11. Compound 16. DiBALH (5.43 mL, 1.0 M in hexanes, 5.43 mmol, 3.00 equiv) was added dropwise to a solution of methyl ester **10** (0.656 g, 1.81 mmol, 1 equiv) in THF (10 mL) at -78 °C. After stirring for 5 min at -78 °C, the reaction mixture was warmed to room temperature and quenched by the addition of methanol (~ 2.5 mL), followed by H_2O (40 mL). After stirring for 10 min, the reaction was extracted with EtOAc (3×40 mL) and the combined organic extracts washed with saturated NaCl (1×25 mL). The organic phase was dried over Na_2SO_4 and was concentrated. Purification by flash column chromatography (30% EtOAc/hexanes) provided 0.56 g (1.61 mmol, 89%) of **16** as a white solid, mp 149–151 °C. 1H NMR ($CDCl_3$): $\delta=7.34$ (dd, 2H, $J=0.8, 8.4$ Hz), 7.18 (s, 2H), m (6.77, 4H), 4.62 (d, 2H, $J=4.4$ Hz), 3.84 (s, 6H), 2.75 (b, 1H), 2.38 (s, 6H). ^{13}C NMR ($CDCl_3$): $\delta=159.13, 158.92, 150.25, 137.27, 133.22, 130.95, 119.01, 115.85, 110.99, 63.55, 55.25, 21.04$. IR (KBr): $\nu=3214$ (b), 2934, 2838, 1606, 1457, 1300. HRMS (EI): calcd for $C_{22}H_{23}NO_3 [M^+]$ 349.1678; found 349.1665. TLC (R_f)=0.15 (30% EtOAc/hexanes).

6.2.12. Compound 17. DMSO (0.25 mL, 3.50 mmol, 2.40 equiv) was added to oxalyl chloride (0.25 mL, 2.90 mmol, 2.00 equiv) in CH_2Cl_2 (15 mL) at -78 °C. After stirring for 5 min, alcohol **16** (0.51 g, 1.45 mmol, 1 equiv) in CH_2Cl_2 (2.5 mL) was added via syringe and the reaction stirred for 5 min at -78 °C. Triethylamine (1.01 mL, 7.25 mmol, 5.00 equiv) was then added and the reaction warmed to room temperature. Upon warming, the solution was diluted with CH_2Cl_2 (50 mL) and washed with H_2O (2×50 mL) and saturated NaCl (1×25 mL). The organic phase was dried over Na_2SO_4 and was concentrated. Purification by flash column chromatography (25% EtOAc/hexanes) provided 0.474 g (1.37 mmol, 94%) of a viscous yellow oil. 1H NMR ($CDCl_3$): $\delta=10.15$ (s, 1H), 7.71 (s, 2H), 7.46 (d, 2H, $J=9.2$ Hz), 6.85 (m, 4H), 3.86 (s, 6H), 2.45 (s, 6H). ^{13}C NMR ($CDCl_3$): $\delta=191.77, 160.52, 159.61, 142.10, 137.47, 132.21, 131.18, 119.91, 116.18, 111.32, 55.31, 21.20$. IR (neat): $\nu=2969, 2838, 2733, 1711$ (s), 1606, 1239, 1178, 1047. HRMS (EI): calcd for $C_{22}H_{20}NO_3$

$[(M-H)^+]$ 346.1443; found 346.1444. TLC (R_f)=0.47 (30% EtOAc/hexanes).

6.2.13. Compound 18. Aldehyde **19** (0.046 g, 0.132 mmol, 1 equiv) and triethylphosphonoacetate (0.033 mL, 0.165 mmol, 1.25 equiv) was suspended in THF (5 mL) and cooled to 0 °C. KO^tBu (0.165 mL, 1.0 M in THF, 0.165 mmol, 1.25 equiv) was added via syringe and the reaction stirred for 10 min at 0 °C. Upon warming to room temperature, the solution was diluted with EtOAc (30 mL) and washed with H₂O (2 × 25 mL) and saturated NaCl (1 × 15 mL). The organic phase was dried over Na₂SO₄ and was concentrated. Purification by flash column chromatography (25% EtOAc/hexanes) provided 0.055 g (0.132 mmol, 100%) of a highly viscous green/yellow oil. ¹H NMR (CDCl₃): δ=7.69 (d, 1H, *J*=15.6 Hz), 7.41 (d, 2H, *J*=9.2 Hz), 7.38 (s, 2H), 6.83 (m, 4H), 6.64 (d, 1H, *J*=16.0 Hz), 4.30 (q, 2H, *J*=6.8 Hz), 3.85 (s, 6H), 2.46 (s, 6H), 1.37 (t, 3H, *J*=6.8 Hz). ¹³C NMR (CDCl₃): δ=165.97, 159.82, 159.36, 142.22, 141.73, 137.33, 132.80, 131.00, 122.27, 119.61, 116.02, 111.16, 60.92, 55.28, 21.11, 14.39. IR (neat): ν=2960, 2838, 1711 (s), 1606, 1239, 1178, 1047. HRMS (MALDI): calcd for C₂₆H₂₈NO₄ [(M-H)⁺] 418.2018; found 418.2024. TLC (R_f)=0.37 (25% EtOAc/hexanes).

6.2.14. Compound 19. Ester **18** (0.115 g, 0.275 mmol, 1 equiv) was suspended in THF (4 mL), LiOH·2H₂O (0.017 g, in 1.0 mL of H₂O, 0.413 mmol, 1.50 equiv) was added and the reaction stirred for 30 min at 23 °C. The reaction mixture was neutralized by the addition of 1 M HCl (0.413 mL, 0.413 mmol, 1.50 equiv) and extracted with CH₂Cl₂ (3 × 25 mL). The organic phase was dried over Na₂SO₄ and was concentrated to afford 0.091 g (0.234 mmol, 85%) of a pure yellow solid. ¹H NMR (CDCl₃): δ=7.78 (d, 1H, *J*=16.4 Hz), 7.42 (d, 2H, *J*=9.2 Hz), 7.39 (s, 2H), 6.83 (m, 4H), 6.65 (d, 1H, *J*=16.0 Hz), 3.85 (s, 6H), 2.46 (s, 6H). ¹³C NMR (CDCl₃): δ=170.58, 159.96, 159.48, 144.43, 141.42, 137.39, 132.61, 131.03, 121.51, 119.85, 116.08, 111.23, 55.32, 21.10. IR (KBr): ν=2934, 2838, 2593, 1711, 1615, 1291, 1248, 1047. HRMS (MALDI): calcd for C₂₄H₂₄NO₄ [(M-H)⁺] 390.1705; found 390.1684.

6.2.15. Compound 20. 2-Bromo-5-methoxytoluene (5.00 g, 24.00 mmol, 1 equiv), *N*-bromosuccinimide (5.13 g, 28.8 mmol, 1.20 equiv), and AIBN (0.08 g, 0.48 mmol, 0.02 equiv) was suspended in benzene (100 mL). The reaction mixture was heated to reflux for 1 h and then cooled to 23 °C. The resulting mixture was filtered and the filtrate was diluted with diethyl ether (75 mL) and washed with H₂O (2 × 100 mL) and saturated NaCl (1 × 50 mL). The organic phase was dried over Na₂SO₄ and was concentrated. The crude solid was triturated with diethyl ether/hexanes (1:4) and filtered to yield 5.50 g (19.60 mmol, 86%) of a white solid, mp 80–82 °C. ¹H NMR (400 MHz, CDCl₃): δ=7.45 (d, 1H, *J*=8.8 Hz), 6.99 (d, 1H, *J*=3.2 Hz), 6.74 (dd, 1H *J*=2.8, 8.8 Hz), 4.55 (s, 2H), 3.80 (s, 3H). IR (KBr): ν=2943, 2847, 1483, 1291, 1256, 1012, 811. TLC (R_f)=0.58 (10% EtOAc/hexanes).

6.2.16. Compound 21. 2-Methoxyethanol (1.13 mL, 14.30 mmol, 2.00 equiv) was added dropwise to a solution of NaH (0.8, 60% w/w in mineral oil, 21.40 mmol,

3.00 equiv) in THF (50 mL) at 0 °C. After stirring for 10 min, benzyl bromide **20** (2.00 g, 7.14 mmol, 1 equiv) in THF (3.0 mL) was added via syringe. The reaction mixture was warmed to RT and stirred for 18 h. The solvent was removed on the rotary evaporator and the residue dissolved in diethyl ether (50 mL), which was subsequently washed with H₂O (2 × 50 mL) and saturated NaCl (1 × 25 mL). The organic phase was dried over Na₂SO₄ and was concentrated. Purification by flash column chromatography (25% EtOAc/hexanes) provided 1.56 g (5.67 mmol, 80%) of a clear oil. ¹H NMR (400 MHz, CDCl₃): δ=7.40 (d, 1H, *J*=8.8 Hz), 7.10 (d, 1H, *J*=3.2 Hz), 6.70 (dd, 1H, *J*=8.8, 3.2 Hz), 4.60 (s, 2H), 3.80 (s, 3H), 3.71 (m, 2H), 3.62 (m, 2H), 3.42 (s, 3H). ¹³C NMR (100 MHz, CDCl₃): δ=158.79, 138.30, 132.72, 114.56, 113.92, 112.40, 72.24, 71.79, 69.92, 59.08, 55.41. IR (neat): ν=2890, 1580, 1475, 1291, 1108. HRMS (MALDI): calcd for C₁₁H₁₅O₃ [(M-Na⁺)] 297.0097; found 297.0094. TLC (R_f)=0.25 (10% EtOAc/hexanes).

6.2.17. Compound 22. *n*-BuLi (5.40 mL, 1.6 M solution in hexanes, 8.60 mmol, 1.20 equiv) was added dropwise to a solution of aryl bromide **21** (1.96 g, 7.14 mmol, 1 equiv) in THF (50 mL) at -78 °C, and the resulting solution stirred for 5 min. Triisopropyl borate (2.16 mL, 9.30 mmol, 1.30 equiv) was added via syringe and the flask warmed to RT. The majority (~75%) of the solvent was removed with the rotary evaporator and 1 M HCl (50 mL) was added and the resulting solution was stirred for 4 h. The mixture was extracted with ether (3 × 33 mL) and the combined organic fractions were extracted with 1 M NaOH (3 × 15 mL). The aqueous extracts were combined and neutralized with HCl (conc.) until acidic to litmus. The aqueous layer was then extracted with EtOAc (3 × 33 mL) and the combined organic phases were dried over Na₂SO₄ and concentrated. This produced a colorless oil (1.20 g, 5.00 mmol, 70%) that hardened upon standing. This material was used in subsequent reactions without further purification. ¹H NMR (400 MHz, CDCl₃): δ=7.88 (d, 1H, *J*=8.4 Hz), 6.89 (dd, 1H, *J*=8.4, 2.4 Hz), 6.81 (d, 1H, *J*=2.4 Hz), 6.27 (b, 2H), 4.63 (s, 2H), 3.83 (s, 3H), 3.65 (m, 2H), 3.55 (m, 2H), 3.37 (s, 3H). IR (KBr): ν=3362 (b), 2917, 1606, 1370, 1265, 1073.

6.2.18. Compound 23. Procedure as for **1** except **22** was used as the boronic acid, P^tBu₃ in THF as the phosphine and CsF as the base. Colorless oil, 52%. ¹H NMR (400 MHz, CDCl₃): δ=7.99 (s, 2H), 7.54 (d, 2H, *J*=8.4 Hz), 7.20 (d, 2H, *J*=2.8 Hz), 6.93 (dd, 2H, *J*=2.8, 8.4 Hz), 4.72 (s, 4H), 3.98 (s, 3H), 3.87 (s, 6H), 3.57–3.54 (m, 8H), 3.35 (s, 6H). ¹³C NMR (100 MHz, CDCl₃): δ=165.83, 160.12, 159.22, 142.50, 137.73, 131.55, 131.42, 120.07, 114.26, 113.45, 71.85, 71.40, 69.61, 59.17, 55.42, 52.73. IR (neat): ν=2890, 1737 (s), 1606, 1248, 1099. HRMS (MALDI): calcd for C₂₉H₃₆NO₈ [(M+H)⁺] 548.2255; found 548.2271. TLC (R_f)=0.20 (45% EtOAc/hexanes).

6.2.19. Compound 23. Procedure as for **16**. Colorless oil, 99%. ¹H NMR (400 MHz, CDCl₃): δ=7.57 (d, 2H, *J*=8.4 Hz), 7.55 (s, 2H), 7.12 (d, 2H, *J*=2.4 Hz), 6.93 (dd, 2H, *J*=2.4, 8.4 Hz), 4.72 (d, 2H, *J*=6.8 Hz), 4.61 (s, 4H), 3.91 (b, 1H), 3.86 (s, 6H), 3.65–3.60 (m, 8H), 3.40 (s, 6H). ¹³C NMR (100 MHz, CDCl₃): δ=159.53, 157.65, 150.80, 136.88, 133.21, 131.36, 119.64, 114.47, 113.59, 72.08, 71.60, 69.60,

63.99, 59.12, 55.41. IR (neat): ν =3441 (b), 2908, 1606, 1431, 1239, 1082, 872. HRMS (MALDI): calcd for $C_{28}H_{36}NO_7 [(M-H)^+]$ 498.2486; found 498.2475. TLC (R_f)=0.19 (60% THF/hexanes).

6.2.20. Compound 24. Procedure as for **17**. Colorless oil, 90%. 1H NMR (400 MHz, $CDCl_3$): δ =10.18 (s, 1H), 7.93 (s, 2H), 7.58 (d, 2H, J =8.4 Hz), 7.18 (d, 2H, J =2.8 Hz), 6.95 (dd, 2H, J =2.8, 8.4 Hz), 4.69 (s, 4H), 3.88 (s, 6H), 3.61–3.54 (m, 8H), 3.36 (s, 6H). ^{13}C NMR (100 MHz, $CDCl_3$): δ =192.30, 159.98, 159.32, 142.51, 137.62, 131.64, 131.39, 120.06, 114.26, 113.48, 71.89, 71.36, 69.63, 59.08, 55.45. IR (neat): ν =2908, 1711 (s), 1615, 1553, 1248, 1099, 889. HRMS (MALDI): calcd for $C_{28}H_{34}NO_7 [(M-H)^+]$ 496.2330; found 496.2318. TLC (R_f)=0.33 (35% EtOAc/hexanes).

6.2.21. Compound 25. A suspension of methyl triphenylphosphonium iodide (0.175 g, 0.433 mmol, 2.90 equiv) in THF (5 mL) was cooled to 0 °C. *n*-BuLi (0.271 mL, 1.60 M in hexanes, 0.433 mmol, 2.90 equiv) was added via syringe and the mixture stirred for 30 min. Aldehyde **24** (0.075 g, 0.151 mmol, 1 equiv) in THF (1 mL) was added via syringe and the reaction stirred for an additional 30 min. The reaction was warmed to RT and stirred for 5 h. The solution was diluted with CH_2Cl_2 (20 mL) and washed with H_2O (2×25 mL) and saturated NaCl (1×10 mL). The organic phase was dried over Na_2SO_4 and was concentrated. Purification by flash column chromatography (45% EtOAc/hexanes) afforded 0.045 g (0.091 mmol, 60%) of **25** as a pale yellow viscous oil. 1H NMR (400 MHz, $CDCl_3$): δ =7.50 (d, 2H, J =8.4 Hz), 7.44 (s, 2H), 7.18 (d, 2H, J =2.4 Hz), 6.91 (dd, 2H, J =2.4, 8.4 Hz), 6.77 (dd, 1H, J =11.2, 17.6 Hz), 6.06 (d, 1H, J =17.6 Hz), 5.51 (d, 1H, J =11.2 Hz), 4.71 (s, 4H), 3.86 (s, 6H), 3.60–3.52 (m, 8H), 3.36 (s, 6H). ^{13}C NMR (100 MHz, $CDCl_3$): δ =159.55, 158.17, 145.12, 137.51, 135.06, 132.58, 131.10, 118.79, 118.31, 113.62, 113.21, 71.89, 71.19, 69.50, 59.05, 55.39. IR (neat): ν =2882, 1597, 1501, 1248, 1099, 1038, 881, 811. HRMS (MALDI): calcd for $C_{29}H_{36}NO_6 [(M-H)^+]$ 494.2537; found 494.2560. TLC (R_f)=0.20 (35% EtOAc/hexanes).

References and notes

- For representative reviews of the chemosensor field, see: (a) Rurack, K.; Resch-Genger, U. *Chem. Soc. Rev.* **2002**, *31*, 116–127. (b) Lavigne, J. J.; Anslyn, E. V. *Angew. Chem. Int. Ed.* **2001**, *40*, 3118–3130. (c) Valeur, B.; Leray, I. *Coord. Chem. Rev.* **2000**, *205*, 3–40. (d) de Silva, A. P.; Eilers, J.; Zlokarnik, G. *Proc. Natl. Acad. Sci. U.S.A.* **1999**, *96*, 8336–8337. (e) Snowden, T. S.; Anslyn, E. V. *Curr. Opin. Chem. Biol.* **1999**, *3*, 740–746. (f) de Silva, A. P.; Gunaratne, H. Q. N.; Gunnlaugsson, T.; Huxley, A. J. M.; McCoy, C. P.; Rademacher, J. T.; Rice, T. E. *Chem. Rev.* **1997**, *97*, 1515–1566. (g) Fabbri, L.; Licchelli, M.; Pallavicini, P.; Sacchi, D.; Taglietti, A. *Analyst* **1996**, *121*, 1763–1768. (h) *Fluorosensors for Ion and Molecule Recognition*. Czarnik, A. W., Ed.; American Chemical Society: Washington, DC, 1994.
- For our previous work on pyridine derived fluorescent chemosensors, see: (a) Mello, J. V.; Finney, N. S. *Angew. Chem. Int. Ed.* **2001**, *40*, 1536–1538. (b) Mello, J. V.; Finney, N. S. *Org. Lett.* **2001**, *3*, 4263–4265. (c) Fang, A. G.; Mello, J. V.; Finney, N. S. *Org. Lett.* **2003**, *5*, 967–970.
- For our previous work on hydrocarbon and Ru(II)bpy₃²⁺ derived chemosensors, see: (a) McFarland, S. A.; Finney, N. S. *J. Am. Chem. Soc.* **2001**, *123*, 1260–1261. (b) McFarland, S. A.; Finney, N. S. *J. Am. Chem. Soc.* **2002**, *124*, 1178–1179. (c) McFarland, S. A.; Finney, N. S. *Chem. Commun.* **2003**, 388–389.
- For an early example of the use of conformational restriction of a binaphthyl to provide a fluorescent response to binding, see: Takeuchi, M.; Yoda, S.; Imada, T.; Shinkai, S. *Tetrahedron* **1997**, *53*, 8335–8348. Note that in this case the maximum reported III_0 was <1.3.
- For recent representative examples, see: (a) Guo, X.; Qian, X.; Jia, L. *J. Am. Chem. Soc.* **2004**, *126*, 2272–2273. (b) Nolan, E. M.; Lippard, S. J. *J. Am. Chem. Soc.* **2003**, *125*, 14270–14271. (c) Walkup, G. K.; Burdette, S. C.; Lippard, S. J.; Tsien, R. Y. *J. Am. Chem. Soc.* **2000**, *122*, 5644–5645.
- For representative examples, see: (a) Ueno, A.; Ikeda, A.; Ikeda, H.; Ikeda, T.; Toda, F. *J. Org. Chem.* **1999**, *64*, 382–387. (b) Metzger, A.; Anslyn, E. V. *Angew. Chem. Int. Ed.* **1998**, *37*, 649–652. (c) Corradini, R.; Dossena, A.; Galaverna, G.; Marchelli, R.; Panagia, A.; Sartor, G. *J. Org. Chem.* **1997**, *62*, 6283–6289. (d) Hamasaki, K.; Usui, S.; Ikeda, H.; Ikeda, T.; Ueno, A. *Supramol. Chem.* **1997**, *8*, 125–135.
- For representative examples of protein/macromolecule FRET based chemosensors, see: (a) Truong, K.; Sawano, A.; Mizuno, H.; Hama, H.; Tong, K. I.; Mal, T. K.; Miyawaki, A.; Ikura, M. *Nat. Struct. Biol.* **2001**, *8*, 1069–1073. (b) Miyawaki, A.; Llopis, J.; Heim, R.; McCaffery, J. M.; Adams, J. A.; Ikura, M.; Tsien, R. Y. *Nature* **1997**, *388*, 882. (c) Adams, S. R.; Harootunian, A. T.; Buechler, Y. J.; Taylor, S. S.; Tsien, R. Y. *Nature* **1991**, *349*, 694. Note that there are numerous FRET based assays for enzymatic activity, etc. that are of great value but do not meet the definition of a chemosensor (see Ref. 1h).
- For representative examples of small molecule FRET based chemosensors, see: (a) Arduini, M.; Felluga, F.; Mancin, F.; Rossi, P.; Tecilla, P.; Tonellato, U.; Valentinuzzi, N. *Chem. Commun.* **2003**, 1606–1607. (b) Schneider, S. E.; O’Neil, S. N.; Anslyn, E. V. *J. Am. Chem. Soc.* **2000**, *122*, 542–543. (c) Pearce, D. A.; Walkup, G. K.; Imperiali, B. *Biorg. Med. Chem. Lett.* **1998**, *8*, 1963–1968. (d) Godwin, H. A.; Berg, J. M. *J. Am. Chem. Soc.* **1996**, *118*, 6514–6515.
- For relevant reviews of Pd-catalyzed cross coupling reactions, see: (a) Miyaura, N.; Suzuki, A. *Chem. Rev.* **1995**, *95*, 2457–2483. (b) Negishi, E.-i. In *Metal-Catalyzed Cross Coupling Reactions*. Diederich, F. Stang, P. J., Eds.; Wiley: New York, 1998. Chapter 1. (c) Suzuki, A. *J. Organomet. Chem.* **1999**, *576*, 147–168.
- While not always required, we find the use of P(*t*-Bu)₃ typically provides the best yields for Suzuki coupling to 2,6-dichloropyridine derivatives. For early reports of the utility of this phosphine, see: (a) Old, D. W.; Wolfe, J. P.; Buchwald, S. L. *J. Am. Chem. Soc.* **1998**, *120*, 9722–9723. (b) Littke, A. F.; Fu, G. C. *Angew. Chem. Int. Ed.* **1997**, *37*, 3387–3388. For the more recent use of this phosphine as its HBF₄ salt, see: Netherton, M. R.; Fu, G. C. *Org. Lett.* **2001**, *3*, 4295–4298.

11. Berlman, I. *Handbook of Fluorescence Spectra of Aromatic Molecules*; Academic: New York, 1971.
12. For the empirical correlation between biaryl dihedral angle and nonradiative decay, see: (a) Fujii, T.; Suzuki, S.; Komatsu, S. *Chem. Phys. Lett.* **1978**, *57*, 175–178. (b) Fujii, T.; Suzuki, S.; Komatsu, S. *Bull. Chem. Soc. Jpn* **1982**, *55*, 2516–2520 and references therein.
13. For general treatments of nonradiative decay, see: (a) Freed, K. F. *Acc. Chem. Res.* **1978**, *11*, 74–80. (b) Klessinger, M.; Michl, J. *Excited States and Photochemistry of Organic Molecules*; VCH: New York, 1995; pp 252–260.
14. For select early derivations of the inverse exponential relationship between energy gap and relaxation rate, see: (a) Engleman, R.; Jortner, J. *Mol. Phys.* **1970**, *18*, 145. (b) Freed, K. F.; Jortner, J. *J. Chem. Phys.* **1970**, *52*, 6272–6291. (c) Siebrand, W. *J. Chem. Phys.* **1967**, *46*, 440–447. This can also be regarded as a restatement of Ermolaev's Rule: Ermolaev, V. L. *Sov. Phys. Usp.* **1963**, *80*, 333–358. *Usp. Fiz. Nauk* **1963**, *80*, 3–40. More quantitatively, $k_{IC} \approx 10^{13} e^{-\alpha \Delta E} \approx 10^{13} f_v$ (where α is a proportionality constant and f_v is the Franck–Condon factor for the transition in question). For energy gaps (ΔE) of ~ 50 kcal/mol, Franck–Condon factors are $\sim 10^5$, leading to $k_{IC} \sim (10^8 \text{ s}^{-1})$. This is slow relative to typical rates of fluorescence emission and ISC, leading to the qualitative $\Delta E \approx 50$ – 60 kcal/mol cutoff for ignoring IC. See: Turro, N. *Modern Molecular Photochemistry*; University Science Books: Sausalito, CA, 1991; pp 180–185.
15. The assertion that the transition dipole should correlate with ground or excited state dipole moment is incorrect at the quantum mechanical level, and inconsistent with some observations (for instance, hexatriene, which has centrosymmetric ground and excited states and thus no net dipole in either state, still has a large ϵ). However, the classical model for oscillator strength equates the transition dipole to the polarizability of a molecule in an applied electric field, which qualitatively relates the ground and excited state dipole moments. As we are comparing molecules of very similar structure, we believe that our argument is at least qualitatively valid. See: Turro, N. *Modern Molecular Photochemistry*; University Science Books: Sausalito, CA, 1991; pp 81–90.
16. The UV spectra suggest that the Einstein coefficient for absorption, and thus the rate of radiative decay, are unchanged. See: Calvert, J. G.; Pitts, J. N. *Photochemistry*; Wiley: New York, 1996; pp 173–174.
17. (a) Rettig, W. *Angew. Chem. Int. Ed.* **1986**, *25*, 971–988. (b) Bhattacharyya, K.; Chowdhury, M. *Chem. Rev.* **1993**, *93*, 507–535.
18. For recent work on the TICT states of simple pyridine derivatives, see: Dobkowski, J.; Wojcik, J.; Kozminski, W.; Kolos, R.; Waluk, J.; Michl, J. *J. Am. Chem. Soc.* **2002**, *124*, 2406–2407 and references therein.
19. While *m*-alkoxy groups are generally considered electron withdrawing due to σ polarization, this generalization is based on ground state phenomena such as electrophilic aromatic substitution. The fact that the excited states are dominantly π^* in nature apparently leads to the *m*-alkoxy groups being moderately electron donating.
20. Lakowicz, J. R. *Principles of Fluorescence Spectroscopy*, 2nd ed.; Kluwer Academic: New York, 1999.
21. Pangborn, A. B.; Giardello, M. A.; Grubbs, R. H.; Rosen, R. K.; Timmers, F. J. *Organometallics* **1996**, *15*, 1518–1520.
22. Li, H.; Jiang, X.; Ye, Y. H.; Fan, C.; Romoff, T.; Goodman, M. *Org. Lett.* **1999**, *1*, 91–93.